A Journal of the Gesellschaft Deutscher Chemiker

Angewandte International Edition GDCh Chemie

www.angewandte.org

Accepted Article

Title: Novel 2D Layered Zinc Silicate Nanosheets with Excellent Photocatalytic Performance for Organic Pollutant Degradation and CO2 Conversion

Authors: Lan Wang, Detlef W. Bahnemann, Liang Bian, Guohui Dong, Jie Zhao, and Chuanyi Wang

To be cited as: *Angew. Chem. Int. Ed.* 10.1002/anie.201903027
Angew. Chem. 10.1002/ange.201903027

Link to VoR: http://dx.doi.org/10.1002/anie.201903027
http://dx.doi.org/10.1002/ange.201903027

WILEY-VCH

10.1002/anie.201903027

WILEY-VCH

Novel 2D Layered Zinc Silicate Nanosheets with Excellent Photocatalytic Performance for Organic Pollutant Degradation and CO_2 Conversion

Lan Wang,* Detlef W. Bahnemann, Liang Bian, Guohui Dong, Jie Zhao, and Chuanyi Wang*

Abstract: Two-dimensional (2D) photocatalysts are highly attractive for their great potential in environmental remediation and energy conversion. Herein, we report a novel layered zinc silicate (LZS) photocatalyst synthesized via liquid-phase epitaxial growth route using silica derived from vermiculite, a layered silicate clay mineral, as both lattice-matched substrate and Si source. The epitaxial growth of LZS is limited in the 2D directions, thus generating the vermiculite-type crystal structure and ultrathin nanosheet morphology with thicknesses of 8~15 nm and lateral size of about 200 nm. Experimental observations and density functional theory (DFT) calculations evince that LZS has a superior band alignment for degradation of organic pollutants and reduction of CO_2 to CO. These nanosheets exhibit efficient photocatalytic performance for 4-chlorophenol (4-CP) degradation and CO_2 conversion to CO, ca. 2.9-fold and 3-fold higher than commercial P25 under UV-vis light, respectively. The present work gives the first example of clay-like 2D photocatalyst with strong photooxidation and photoreduction capabilities.

Semiconductor photocatalysis is considered to be one of the most promising and practical solutions to address current and future energy and environmental concerns.[1] Since the discovery of water-splitting system based on titanium dioxide (TiO_2) under light irradiation,[2] various inorganic materials have been explored as catalysts for photocatalysis, aiming to produce H_2 and O_2 from water,[3] produce hydrocarbon fuels through the conversions of CO_2 with H_2O,[1b, 4] and eliminate organic pollutants.[5] Among various inorganic photocatalysts, two dimensional (2D) nanosheet-shaped materials as novel photocatalysts, particularly those having layered structure, have been of great interest due to their diverse morphological advantages such as high surface-to-volume ratio, relatively short travel distance of the photoexcited carriers, abundant surface active sites, and interlayer space for hybridization with other species[6], all of which are beneficial to photocatalytic reactions compared with the powdered photocatalysts.

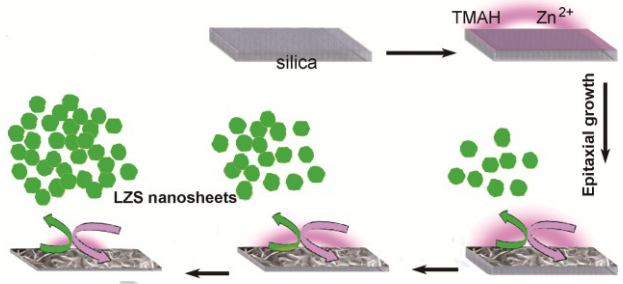

Scheme 1. Schematic illustration of liquid-phase epitaxial growth of LZS nanosheets in hydrothermal condition.

Layered silicates as typical 2D inorganic materials were widely used as catalyst supports as well as adsorbents, owing to their low cost and abundant reserves.[7] So far, however, the photocatalytic properties of these materials have been mostly ignored due to their photo-inert in nature. For natural layered silicates, such as clay minerals (e.g., vermiculite, montmorillonite, etc.), their crystal structure consists of layers made up of two silicon-oxygen tetrahedra sheets fused to an edge-shared octahedral sheet of either aluminum or magnesium hydroxide.[8] Indeed, they have no photocatalytic activity under UV irradiation. With the consideration that the synthetic layered silicates can be incorporated with transition metals in the octahedral position, metal silicates with layered structure will be envisioned as providing the opportunity of having silicate-based photocatalysts.

ZnO as a wide band gap semiconductor has been widely used in the photocatalytic degradation. From a crystallographic point of view, Zn(II) can be incorporated into the octahedral framework of silicates.[9] Moreover, Zn-type layered double hydroxides (e.g. ZnAl LDH, ZnCr LDH and ZnTi LDH), a known class of anionic clays, have been used as photocatalysts for reduction of CO_2,[10] and degradation of organic dyes and pesticides,[11] respectively. We expect that the structure and performance advantages of LDH derived from zinc can be applied to the clay-type 2D layered silicates material. Accordingly, when the transition metal Zn(II) is present in well-defined structural position, the obtained layered zinc silicate is expected to overcome the instability of ZnO in aqueous system and retain its photocatalytic activity. In many cases, however, the presence of non-homogenous nanometer-scale morphology and the high concentration of crystalline impurities

[*] Dr. L. Wang, Laboratory of Environmental Sciences and Technology, Xinjiang Technical Institute of Physics & Chemistry; Key Laboratory of Functional Materials and Devices for Special Environments, Chinese Academy of Sciences, Urumqi 830011, China
E-mail: wanglan@ms.xjb.ac.cn
Prof. C.Y. Wang, Dr. G.H. Dong, Dr. J. Zhao, School of Environmental Science and Engineering, Shaanxi University of Science and Technology, Xian 710021, China
E-mail: cywang@ms.xjb.ac.cn
Prof. D. W. Bahnemann, Laboratorium fur Nano- und Quantenengineering, Leibniz Universität Hannover, Schneiderberg 39, 30167 Hannover, Germany
Dr. L. Bian, Key Laboratory of Solid Waste Treatment and Resource Recycle, South West University of Science and Technology, Mianyang 621010, China

Supporting information for this article is given via a link at the end of the document.

on the layered zinc silicate is likely the primary hindrance to being used as a photocatalytic material.[12] Thus, we envisioned that if the 2D silica (tetrahedral SiO_4 units) derived from nature clay minerals could be used as the source of silicon, which would endow the obtained materials with excellent photocatalytic properties.

Considering the toxic gradient of major pollutants, chlorinated phenolic compounds represent a serious threat to the aquatic ecological system due to their toxicity and resist biodegradation. Among the chlorinated phenolic compounds, 4-chlorophenol (4-CP) is a kind of typical toxic chlorinated compound, which has direct effect on the environmental pollution and has been the subject of numerous recent studies,[13] thus it was selected as a model nondye organic pollutant. The present investigation is directed toward the synthesize of layered zinc silicate (LZS) nanosheets using activated silica derived from vermiculite as both substrate and silicon source via a epitaxial growth in hydrothermal condition (Scheme 1, experimental details are given in Supporting Information (SI)). As-synthesized LZS exhibits high activities for the photocatalytic degradation of 4-CP and the photoreduction of CO_2 to CO. To the best of our knowledge, it is the first time to show that crystalline LZS nanosheets were synthesized chemically to obtain highly active photocatalysts for organic pollutants elimination and energy conversion.

Powder X-ray diffraction (XRD) pattern of LZS indicates the formation of layered phase (Figure 1a), which is similar to some other synthetic clay minerals.[12b, 14] Very broad XRD peaks in the range of 5-65° that could be indexed to the vermiculite structure zinc silicate. Reflections at 14.2 Å (6.2° 2θ), 7.1 Å (12.4° 2θ), 4.6 Å (19.5° 2θ), 3.5 Å (25.4° 2θ), 2.7 Å (33.7° 2θ) and 1.5 Å (60.2° 2θ) correspond to the (001), (002), (110, 020), (004), (130, 200), and (060, 330) plane of LZS, respectively. The position of the (060, 330) reflection at 1.5 Å confirms a trioctahedral structure for the layered silicate similar to natural vermiculite, and the (001) reflection at 14.2 Å signifies the special distance between two sheets. Chemical analysis indicates that the synthetic LZS is mainly Zn and Si in composition (Table S2). The calculated composition of the unit cell and the lattice parameters of LZS are shown in Table S3. LZS crystallizes in a monoclinic crystal system, space group C2/m, as shown in Figure 1b. Thus, it may be deduced from these data that the LZS is a vermiculite-type layered silicate.[15] The silicate layer of LZS is composed of zinc oxide octahedral sheet sandwiched between two tetrahedral sheets of silica. The layer negative charges originates from a minor fraction of isomorphic substitution of Al^{3+} for Si^{4+} in the tetrahedral sheets, which are compensated by interlayer cation Mg^{2+}. Accordingly, the multilayered structure of LZS is stabilized by the interaction between the species in the interlayer space and the negatively charged layer, as well as hydrogen bonds from water molecules.

Scanning electron microscopy (SEM) image of LZS film clearly shows that the nanoplates with high density are grown uniformly on the silica substrate (Figure 1c), whose ab-plane is almost perpendicular to the substrate. These LZS nanocrystals can desquamated automatically from substrate, and the resulting sample displays uniform plate-like nanocrystals with a lateral size of about 200 nm and an ultrathin thickness of about 10 nm (Figure 1d). Further transmission electron microscopy

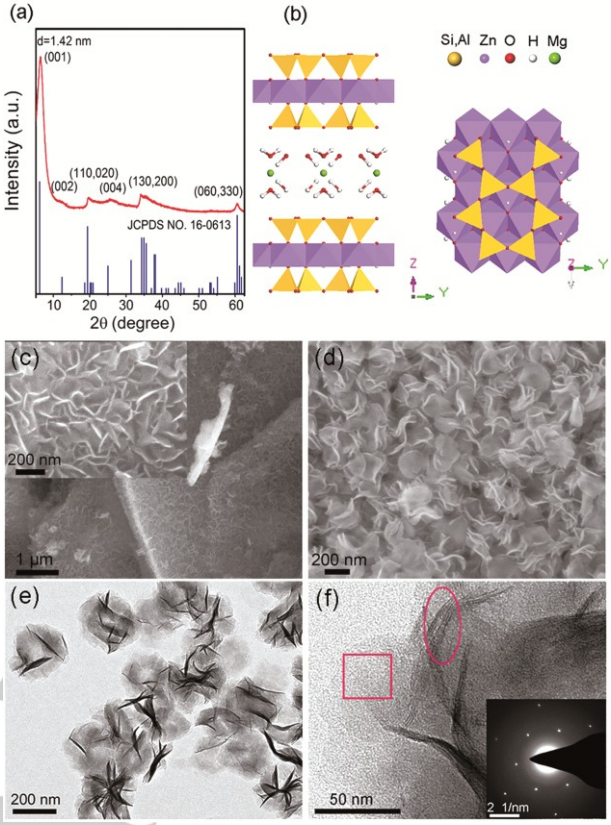

Figure 1. (a) XRD pattern of LZS, and standard peak positions and intensities accordingly marked for vermiculite (JCPDS No. 16-0613). (b) Polyhedral models of the LZS structure as seen from the [100] and [001] directions. SEM images of (c) LZS epitaxial film grown on silica substrate, and (d) LZS nanosheets peeled from silica substrate in the reaction process. (e) TEM image of LZS nanosheets. (f) High-magnification view of (e) (ellipse lines mark the layered structure of upstanding nanoplates), and SAED pattern recorded along the [001] axis on a lying nanoplate indicated by the square region in f (inset).

(TEM) analysis shows that the LZS has thin two-dimensional (2D) nature of the plate-like nanostructures (Figure 1e), where the near transparency to the electron beams indicates the ultrathin nature. A representative high-magnification image (Figure 1f) of the curled edge or upstanding platelets shows the LZS is composed of 5-8 layers with a thickness distribution of 8-15 nm, a ~1 nm thickness of monolayer thickness, and an interlayer spacing of about 1.4 nm, which is in agreement with the result of XRD analysis. The selected area electron diffraction (SAED) pattern (Figure 1f, inset) was obtained from one lying platelet, where the hexagonally arranged spots confirm the single crystal nature and typical hexagonal structure, which is in good agreement with the typical hexagonal structure of vermiculite.[16] Obviously, the same silica phases of LZS and substrate imply that they are sufficiently lattice-matched to allow epitaxial growth of the LZS sheets on the silica substrate surface.

The X-ray photoelectron spectroscopy (XPS) peaks for the O_{1s}, Si_{2p} and Zn_{2p} states are provided in Figure S1. The O_{1s} peak can be deconvoluted into three peaks: two main peaks at 532.5 eV and 531.8 eV, and a small shoulder located at about 532.3 eV. The former two peaks may be assigned to the Si-O-Si bond and O-Zn bond, respectively, and the latter is resulted from the -

O-H bond on LZS.[17] The $Zn_{2p3/2}$ signal of LZS shows a symmetric peak centered at 1022.4 eV, which is the same as that the reported earlier for zinc silicate (hemimorphite).[18] The Si_{2p} binding energy in LZS is 103.1 eV, close to the value observed for a silicate.[19] However, the value is higher than that of the natural phyllosilicates,[20] which might correspond to the electron environments of zinc in the octahedral structural site. ^{29}Si MAS nuclear magnetic resonance (NMR) spectrum of LZS is displayed in Figure S2. The LZS shows a major peak at -96.4 ppm with a shoulder at -86.8 ppm, corresponding to Q^3 (0Al) units and Q^3 (1Al), respectively.[14b, 21] Q^3 means the associated number of units of sheet silicate structures, compatible with some structures of zincsilite and vermiculite.[12a, 21]

UV-vis diffuse reflectance spectrum (DRS) shows that the absorption edge of the LZS is around 355 nm (Figure 2a). According to the Kubelka-Munck plot (Figure 2a, inset), the direct band-gap is estimated to 3.5 eV. To estimate that valence band maximum (VBM) position of LZS, the VB XPS analysis and Mott-Schottky experiment were performed (Figure S3). The VBM position of LZS was estimated to be 2.9 V. According to its optical band gap, the corresponding conduction band minimum (CBM) position was then estimated to be -0.6 V.[22] Based on the above two experimental results in combination, the band diagram of LZS is schematically expressed in comparison with the potentials for CO/CO_2, $O_2^{-\bullet}/O_2$ and $H_2O/\cdot OH$, respectively, in the NHE scale (Figure 2b).

DFT calculation was performed to obtain insight into the electronic structure of LZS. The calculated electronic band structure, the total density of states (TDOS) and the partial density of states (PDOS) are displayed in Figure S4 and Figure 2c. It was found that VBM and CBM of LZS are located at the same V point with a direct energy gap of about 3.9 eV, wider than the experimental values of 3.5 eV but within a 0.4 eV deviation. The DOS peaks show that the VB top is mainly composed of Zn 3d and O 2p orbitals, and the CB bottom is mainly constructed by O 2p and Zn 4s. In the bottom of the conduction band, impurity levels which mainly come from Mg 3s state appear.

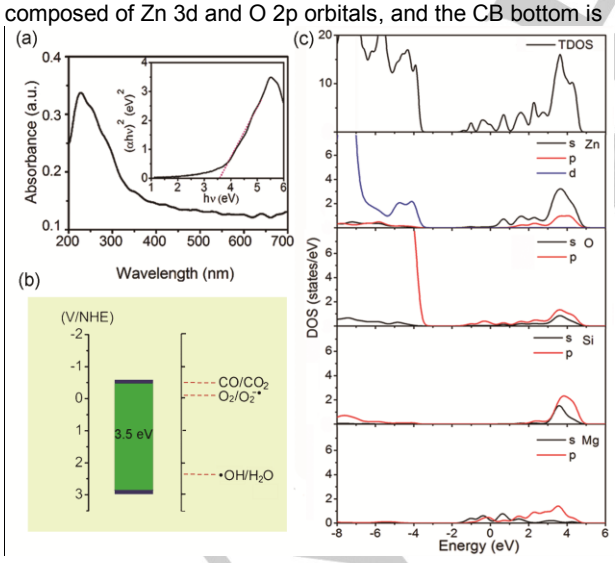

Figure 2. (a) UV-vis absorption spectrum (inset: plot of $(\alpha h\nu)^2$ vs hν) and (b) schematic band structure of LZS. (c) Total density of states (TDOS) and partial density of states (PDOS) for LZS.

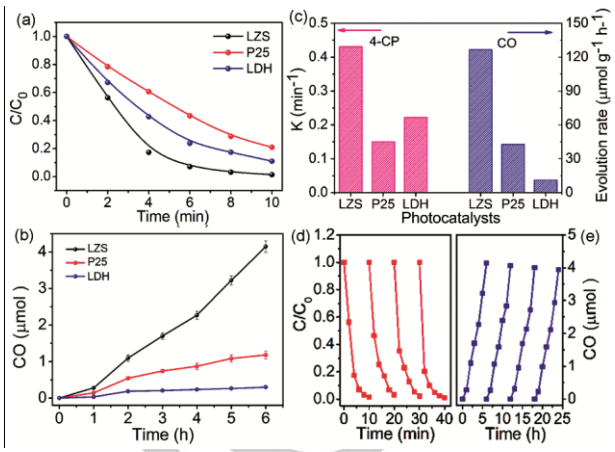

Figure 3. Time courses of 4-CP degradation (a) and CO evolution (b) by LZS, ZnAl-LDH, and P25 under simulated sunlight irradiation. (c) Reaction rate of photodegradation of 4-CP and CO evolution rate from the photocatalytic CO_2 reduction on photocatalysts. Stabilities of LZS during the photocatalytic degradation of 4-CP (d) and photocatalytic CO_2 reduction (e).

The photocatalytic performance of LZS was tested in two types of reactions: photocatalytic degradation of 4-CP, and photoreduction of CO_2 under UV-visible light. ZnAl-layered double hydroxide (ZnAl-LDH, Figure S5) and commercial TiO_2 (P25) are employed as references for comparison. The pseudo-first order rate constant shown in Figure 3c derived from the degradation data in Figure 3a is used to evaluate the photocatalytic oxidation activity. Obviously, LZS, with a large S_{BET} of 185.4 $m^2 \cdot g^{-1}$, is more active than ZnAl-LDH and P25 under UV-visible irradiation. The 4-CP degradation rate of LZS is 2-fold of ZnAl-LDH and 2.9-fold of P25. Photocatalytic conversion of CO_2 with H_2O vapor was conducted under UV-vis light and the results are shown in Figures 3b and 3c. In addition to oxygen, CO was found to be the major reduction product, consistent with previous report.[23] LZS exhibits stable CO evolution at a rate of 126.7 $\mu mol \cdot g^{-1} \cdot h^{-1}$, whereas LDH and P25 produce CO at 11.2 $\mu mol \cdot g^{-1} \cdot h^{-1}$ and 42.7 $\mu mol \cdot g^{-1} \cdot h^{-1}$ under the same conditions, respectively. Tables S4 and S5 summarize the performances of some widely used layered photocatalysts and typical TiO_2 powder photocatalysts for the photocatalytic degradation of 4-CP and the photoreduction of CO_2, respectively. These results suggest that LZS is extremely efficient for the 4-CP removal and CO_2 photoreduction without using noble metal co-catalysts such as Au or Pt. In this stability tests, LZS shows no obvious deactivation in photocatalytic activity for the degradation of 4-CP and CO production after 4 cycles (Figures 3d and 3e). The crystal and morphological structures of LZS are very well kept after the photocatalytic reactions (Figure S6). The wavelength-dependent apparent quantum yield (AQY) (Figure 4a) decrease with increasing the wavelength of incident light, which is consistent with the optical absorption of LZS, implying the chemical processes of photodegradation and photoreduction are primarily driven by the photoinduced carrier of LZS.[24] Thus,

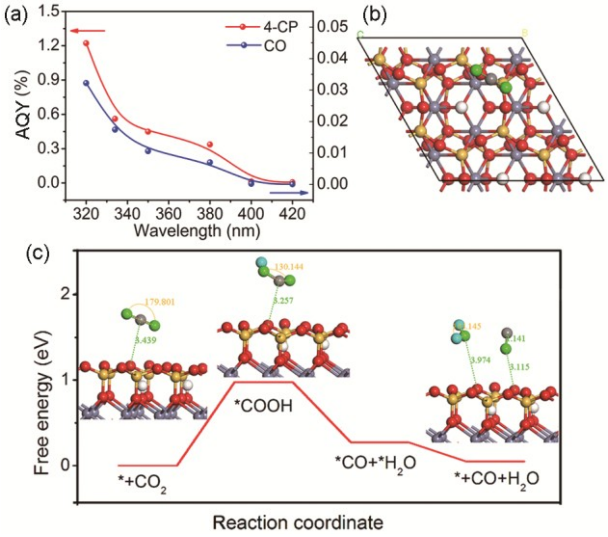

Figure 4. (a) Wavelength-dependent apparent quantum yield (AQY) of 4-CP photodegradation and CO_2 photoreduction over LZS at various incident light wavelengths. (b) Top view of the optimized structure of CO_2 adsorption on LZS sheet. (c) Free energy diagram for the reduction of CO_2 to CO on LZS (001). The local configurations of the adsorbates on the LZS sheet at initial state (IS), transition state (TS), and final state (FS) along the minimum-energy pathway are shown in the inserts, respectively. (C, O and H atoms of the adsorbates are represented by grey, light green and light blue spheres).

we can conclude that LZS is a superior catalyst in both photocatalytic degradation of organics and CO_2 photoreduction.

Hydroxyl radicals (•OH) and superoxide radicals ($O_2^{-\bullet}$) are generally considered as important reactive oxygen species (ROS) in photodegradation of organic pollutants. Here, we employed the electron paramagnetic resonance (EPR) spin-trap technique (with DMPO) to confirm the generation of both •OH and $O_2^{-\bullet}$ radicals (Figure S7).[25] DMPO-•OH with a typical EPR spectrum of four-line with intensity ratio of 1:2:2:1 and DMPO-$O_2^{-\bullet}$ with six characteristic peaks were obviously observed in the suspension of LZS under irradiation, whereas no such signals were detected for the samples without irradiation. The redox potential for $O_2/O_2^{-\bullet}$ is -0.16 V, and for H_2O/•OH is 2.32 V.[26] The energy levels of the conduction band and the valence band were -0.6 and +2.9 eV for LZS, respectively. Apparently, in the case of LZS, the photoexcited holes in valence band and electrons in conduction band have sufficient energy to oxidize/reduce the oxygen containing species to form corresponding ROS.

Hydroquinone (HQ), benzoquinone (BQ), hydroxybenzoquinone(HBQ), and 4,4-oxydiphenol have been found to be the main intermediates of the photocatalytic 4-CP degradation over LZS (Table S6), but no 4-chlorocatechol (4-CC) product is observed, in part, which is different from that over P25.[27] The photodegradation pathways are proposed as shown in Figure S8. In the presence of LZS, BQ can be formed by the reaction of hydroxy phenyl radical (HPR) with superoxide radicals or by the oxidation of HQ, and then be oxidized to HBQ by hydroxyl radical. HBQ and 4,4-oxydiphenol then undergo further oxidation to induce ring cleavage to form aliphatic intermediates, and finally, they are degraded to CO_2 and H_2O. The mechanistic differences of photocatalytic reactions can also reflect the distinctions of chemical nature between LZS and P25 in generating e^- and h^+, as well as reactive oxygen species.

In addition, the conduction band edge is also reasonably well aligned with the CO_2 to CO potential under UV-vis illumination. The potential for reducing CO_2 vs NHE in water at a pH value of 7 is given in equation 1. The standard reduction potential of CO_2 to CO occurs at -0.53 V.[1b, 28] The relative energies and the electrons required for this reduction reaction indicate that CO could be the preferred product of photoreduction of CO_2, which can be attributed to the suitable electron reduction ability of the LZS.[29]

$$CO_2 + 2H^+ + 2e^- \rightarrow CO + H_2O, \quad E^0_{redox} = -0.53V \qquad \text{Eq. (1)}$$

To gain further insights into the catalytic mechanism for reducing CO_2 to CO over LZS, we performed DFT calculation to determine the catalytic reactions associated with the LZS structure. It has been known that the CO_2 reduction reactions usually occur on the surface of the photocatalysts.[23] The layered structure of LZS creates an ideal 2D architecture that allows engineered surface with active sites ratio approaching 100%, thus surface oxygen can be suggested to be the active site for CO_2 reduction. A similar result is also reported for the CO_2 interaction with the (001) surface of anatase TiO_2.[30] DFT calculation based on the LZS structure model was employed to investigate the possible reaction pathway along with the local configurations (Figures 4b and 4c). It has been known that the adsorbed *COOH formation is usually a key step in the reduction process of CO_2 to CO.[31] The corresponding free energy barrier of 1.01 eV for *COOH should be overcome in the present reaction over LZS, which is close to the value for other metal-free system.[32]

In summary, a novel layer-structured photocatalyst consisting of zinc silicate nanosheet ($Mg_{0.1}Zn_6(Si_{7.9}Al_{0.1})O_{20}(OH)_4 \bullet nH_2O$) has been successfully synthesized by liquid-phase epitaxial growth route for the first time, in which 2D silica serves as both Si source and 2D template with suitable lattice parameters for the formation of continuous zinc silicate films. These nanosheets are typical 2D nanomaterials with a vermiculite-type structure and platelet thicknesses of about 10 nm which corresponds to five reproducible stacking layers, exhibiting high photocatalytic activity and good stability for 4-CP degradation and the conversion of CO_2 into CO in the presence of water vapor. Experimental and theoretical studies support that the excellent performance should be ascribed to the ideal 2D architecture allowing engineered surface with high active sites ratio, the large specific surface areas, the very positive VB and negative CB positions, which endows it with a highly strong photooxidation ability to produce •OH radicals and photoreduction ability. To our knowledge, it is the first report that clay-like 2D materials display two photocatalytic activities. This work not only demonstrates layered zinc silicate system could be a potential candidate for photocatalysis, but may also inspire the development of high-performance 2D nanomaterials for catalysis, and other potential applications.

Acknowledgements

Financial support by the National Nature Science Foundation of China (Grant Nos. U1703129, 41872039 and 21876104) is gratefully acknowledged.

Keywords: layered zinc silicate • nanosheets • photocatalysis • 4-chlorophenol degradation • CO_2 reduction

[1] a) X. Chen, S. S. Mao, *Chem. Rev.* **2007**, 107, 2891-2959; b) S. N. Habisreutinger, L. Schmidt-Mende, J. K. Stolarczyk, *Angew. Chem. Int. Edit.* **2013**, 52, 7372-7408; c) U. I. Gaya, A. H. Abdullah, *J. Photoch. Photobio. C* **2008**, 9, 1-12.

[2] A. Fujishima, K. Honda, *Nature* **1972**, 238, 37.

[3] A. Kudo, Y. Miseki, *Chem. Soc. Rev.* **2009**, 38, 253-278.

[4] a) X. Li, J. Q. Wen, J. X. Low, Y. P. Fang, J. G. Yu, *Sci. China Mater.* **2014**, 57, 70-100; b) T. Oshima, T. Ichibha, K. S. Qin, K. Muraoka, J. J. M. Vequizo, K. Hibino, R. Kuriki, S. Yamashita, K. Hongo, T. Uchiyama, K. Fujii, D. L. Lu, R. Maezono, A. Yamakata, H. Kato, K. Kimoto, M. Yashima, Y. Uchimoto, M. Kakihana, O. Ishitani, H. Kageyama, K. Maeda, *Angew. Chem. Int. Edit.* **2018**, 57, 8154-8158.

[5] a) A. Di Paola, E. Garcia-Lopez, G. Marci, L. Palmisano, *J. Hazard. Mater.* **2012**, 211, 3-29; b) H. Kisch, *Angew. Chem. Int. Edit.* **2013**, 52, 812-847; c) J. W. Tang, Z. G. Zou, J. H. Ye, *Angew. Chem. Int. Edit.* **2004**, 43, 4463-4466.

[6] a) S. Park, H. J. Song, C. W. Lee, S. W. Hwang, I. S. Cho, *Acs Appl. Mater. Inter.* **2015**, 7, 21860-21867; b) S. Ida, T. Ishihara, *J. Phys. Chem. Lett.* **2014**, 5, 2533-2542; c) J. X. Low, S. W. Cao, J. G. Yu, S. Wageh, *Chem. Commun.* **2014**, 50, 10768-10777.

[7] a) J. Liu, G. K. Zhang, *Phys. Chem. Chem. Phys.* **2014**, 16, 8178-8192; b) Y. Ide, N. Ochi, M. Ogawa, *Angew. Chem. Int. Edit.* **2011**, 50, 654-656; c) Y. Ide, M. Torii, T. Sano, *J. Am. Chem. Soc.* **2013**, 135, 11784-11786; d) S. D. Miao, Z. M. Liu, B. X. Han, J. Huang, Z. Y. Sun, J. L. Zhang, T. Jiang, *Angew. Chem. Int. Edit.* **2006**, 45, 266-269; e) Y. Kuwahara, D. Y. Kang, J. R. Copeland, N. A. Brunelli, S. A. Didas, P. Bollini, C. Sievers, T. Kamegawa, H. Yamashita, C. W. Jones, *J. Am. Chem. Soc.* **2012**, *134*, 10757-10760.

[8] M. F. Brigatti, E. Galan, B. K. G. Theng, in *Structures and mineralogy of clay minerals*, Vol. 1, chap. 2 (Eds.: F. Bergaya, B. K. G. Theng, G. Lagaly), Elsevier, Amsterdam, **2006**, pp. 25-44.

[9] V. Luca, D. J. Maclachlan, R. F. Howe, R. Bramley, *J. Mater. Chem.* **1995**, 5, 557-564.

[10] L. Mohapatra, K. Parida, *J. Mater. Chem. A.* **2016**, 4, 10744-10766.

[11] a) J. L. White, M. F. Baruch, J. E. Pander, Y. Hu, I. C. Fortmeyer, J. E. Park, T. Zhang, K. Liao, J. Gu, Y. Yan, T. W. Shaw, E. Abelev, A. B. Bocarsly, *Chem. Rev.* **2015**, 115, 12888-12935; b) Y. F. Zhao, X. D. Jia, G. I. N. Waterhouse, L. Z. Wu, C. H. Tung, D. O'Hare, T. R. Zhang, *Adv. Energy Mater.* **2016**, 6.

[12] a) J. Qu, C. Y. Cao, Y. L. Hong, C. Q. Chen, P. P. Zhu, W. G. Song, Z. Y. Wu, *J. Mater. Chem.* **2012**, 22, 3562-3567; b) J. Qu, Y. Yan, Y. X. Yin, Y. G. Guo, W. G. Song, *Acs Appl. Mater. Inter.* **2013**, 5, 5777-5782.

[13] a) C. Guillard, J. Disdier, C. Monnet, J. Dussaud, S. Malato, J. Blanco, M. I. Maldonado, J. M. Herrmann, *Appl. Catal. B-Environ.* **2003**, 46, 319-332; b) S. Y. Lan, J. X. Feng, Y. Xiong, S. H. Tian, S. W. Liu, L. J. Kong, *Environ. Sci. Technol.* **2017**, 51, 6560-6569; c) Y. Hou, J. Yang, C. J. Lei, B. Yang, Z. J. Li, Y. Xie, X. W. Zhang, L. C. Lei, J. H. Chen, *Acs Sustain. Chem. Eng.* **2018**, 6, 6497-6506.

[14] a) C. S. Pascua, M. Ohnuma, Y. Matsushita, K. Tamura, H. Yamada, J. Cuadros, J. H. Ye, *Appl. Clay Sci.* **2010**, 48, 55-59; b) K. A. Carrado, R. Csencsits, P. Thiyagarajan, S. Seifert, S. M. Macha, J. S. Harwood, *J. Mater. Chem.* **2002**, 12, 3228-3237.

[15] P. G. Slade, P. G. Self, J. P. Quirk, *Clay Clay Miner.***1998**, 46, 629-635.

[16] L. Wang, X. Wang, J. Yin, C. Y. Wang, *Appl. Clay Sci.* **2016**, 132, 17-23.

[17] a) C. X. Gui, Q. Q. Wang, S. M. Hao, J. Qu, P. P. Huang, C. Y. Cao, W. G. Song, Z. Z. Yu, *Acs Appl. Mater. Inter.* **2014**, 6, 14653-14659; b) Y. Liu, J. M. Shen, Z. L. Chen, L. Yang, Y. Liu, Y. Han, *Appl Catal a-Gen* **2011**, 403, 112-118.

[18] Z. L. Yin, Z. Y. Ding, H. P. Hu, K. Liu, Q. Y. Chen, *Hydrometallurgy* **2010**, 103, 215-220.

[19] B. Carriere, J. P. Deville, D. Brion, J. Escard, *J. Electron. Spectrosc.* **1977**, 10, 85-91.

[20] a) C. Mosser, A. Mosser, M. Romeo, S. Petit, A. Decarreau, *Clay Clay Miner.* **1992**, 40, 593-599; b) J. F. Moulder, W. F. Strckle, P. E. Sobol, K. D. Bomben, (Ed.: J. Chastain), *Physical Electronics*, Inc., **1995**, p. 201.

[21] C. A. Weiss, S. P. Altaner, R. J. Kirkpatrick, *Am. Mineral.* **1987**, 72, 935-942.

[22] K. Chang, M. Li, T. Wang, S. X. Ouyang, P. Li, L. Q. Liu, J. H. Ye, *Adv. Energy Mater.* **2015**, 5.

[23] Y. F. Zhao, G. B. Chen, T. Bian, C. Zhou, G. I. N. Waterhouse, L. Z. Wu, C. H. Tung, L. J. Smith, D. O'Hare, T. R. Zhang, *Adv. Mater.* **2015**, 27, 7824-7831.

[24] Y. X. Li, S. X. Ouyang, H. Xu, X. Wang, Y. P. Bi, Y. F. Zhang, J. H. Ye, *J. Am. Chem. Soc.* **2016**, 138, 13289-13297.

[25] a) Y. Nosaka, A. Y. Nosaka, *Chem. Rev.* **2017**, 117, 11302-11336; b) Y. Lu, H. T. Yu, S. Chen, X. Quan, H. M. Zhao, *Environ. Sci. Technol.* **2012**, 46, 1724-1730.

[26] P. M. Wood, *Biochem. J.* **1988**, 253, 287-289.

[27] a) J. Theurich, M. Lindner, D. W. Bahnemann, *Langmuir* **1996**, 12, 6368-6376; b) J. H. Clark, M. S. Dyer, R. G. Palgrave, C. P. Ireland, J. R. Darwent, J. B. Claridge, M. J. Rosseinsky, *J. Am. Chem. Soc.* **2011**, 133, 1016-1032.

[28] K. Teramura, S. Iguchi, Y. Mizuno, T. Shishido, T. Tanaka, *Angew. Chem. Int. Edit.* **2012**, 51, 8008-8011.

[29] Z. Y. Sun, N. Talreja, H. C. Tao, J. Texter, M. Muhler, J. Strunk, J. F. Chen, *Angew. Chem. Int .Edit.* **2018**, 57, 7610-7627.

[30] a) L. Mino, G. Spoto, A. M. Ferrari, *J. Phys. Chem. C* **2014**, 118, 25016-25026; b) K. Li, B. S. Peng, T. Y. Peng, *Acs Catal.* **2016**, 6, 7485-7527.

[31] D. F. Gao, H. Zhou, J. Wang, S. Miao, F. Yang, G. X. Wang, J. G. Wang, X. H. Bao, *J. Am. Chem. Soc.* **2015**, 137, 4288-4291.

[32] H. P. Yang, Y. Wu, Q. Lin, L. D. Fan, X. Y. Chai, Q. L. Zhang, J. H. Liu, C. X. He, Z. Q. Lin, *Angew. Chem. Int. Edit.* **2018**, 57, 15476-15480.

10.1002/anie.201903027

WILEY-VCH

Entry for the Table of Contents

COMMUNICATION

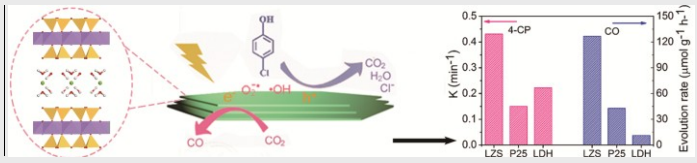

Lan Wang, Detlef W. Bahnemann, Liang Bian, Guohui Dong, Jie Zhao, and Chuanyi Wang**

Page No. – Page No.

Novel 2D Layered Zinc Silicate Nanosheets with Excellent Photocatalytic Performance for Organic Pollutant Degradation and CO_2 Conversion

Ultrathin layered zinc silicate (LZS) nanosheet was synthesized via liquid-phase epitaxial growth route by incorporating Zn into the octahedra sheet of layered silicates. The obtained LZS has a superior band alignment for strong photooxidation and photoreduction capabilities, thus exhibiting excellent photocatalytic performance for 4-chlorophenol degradation and CO_2 conversion to CO.